

1

Introduction

The so-called Λ Cold Dark Matter (Λ CDM) model is currently the most widely accepted theory for the structure and evolution of the Universe. A combination of experimental data involving the power spectrum of the Cosmic Microwave Background (CMB) radiation temperature fluctuations, the abundance and weak-lensing mass measurements of galaxy clusters, the Type Ia supernovae magnitude-redshift relation and large scale structure observations has placed strong constraints on the free parameters of this cosmological model [1].

In the framework of Λ CDM cosmology, the large scale structure of the Universe is assumed to be homogeneous and isotropic – denoted as “cosmological principle” – on scales of the order of 100 Mpc. Therefore, the local inhomogeneities can be treated as perturbations to the general homogeneity of the Universe, and it is represented by the Friedmann–Robertson–Walker metrics. The evolution with time of this model universe is described by

$$\left(\frac{dR(t)}{dt}\right)^2 = -kc^2 + \frac{(8\pi G\rho(t) + \Lambda)R(t)^2}{3} \quad (1.1)$$

$$\frac{d(\rho(t)c^2 R(t)^3)}{dt} = -p \frac{dR(t)^3}{dt} \quad (1.2)$$

as obtained from the field equations of general relativity. Here, k denotes the spatial curvature, dt the cosmic time separation, ρ the density of matter plus radiation. $R(t)$ is the so-called cosmic scale factor that describes the expansion (or contraction) of the Universe. It has the dimensions of a distance and is dependent on the cosmic time t . The constant k is defined in a way that $k = +1$ for a positive spatial curvature, $k = 0$ for a flat space and $k = -1$ for a negative curvature. The cosmic time is defined by standard clocks comoving with the cosmic fluid. If one sets t to the same value for all clocks when a local property of the cosmic fluid, for example, the average local density of matter, has attained a certain agreed value, by virtue of the cosmological principle, the same value of that property (possibly different from the one at the time of synchronization) has to be measured whenever clocks show the same time.

Equation (1.1) includes the cosmological constant Λ . If Λ were to vary with t , it represents a so-called “dark energy”. Current observations are consistent with Λ

being a constant.¹⁾ The evolution of $R(t)$ is controlled by ρ , the geometry k and Λ . By defining the function $H(t)$ as

$$H(t) \equiv \frac{dR(t)}{dt} \frac{1}{R(t)} \quad (1.3)$$

one can rewrite Eq. (1.1) as

$$H(t)^2 = -\frac{k c^2}{R(t)^2} + \frac{8\pi G \rho(t)}{3} + \frac{\Lambda}{3} \quad (1.4)$$

The value of $H(t)$ determined today is the Hubble constant H_0 . It is customary to introduce the critical density $\rho_c \equiv 3H(t)^2/(8\pi G)$ and define the density parameter $\Omega_\rho = \rho/\rho_c$, an equivalent for the cosmological constant $\Omega_\Lambda = \Lambda/(3H(t)^2)$, and the sum $\Omega = \Omega_\rho + \Omega_\Lambda$. With these definitions, Eq. (1.4) becomes

$$(1 - \Omega)H(t)^2 R(t)^2 = -k c^2 \quad (1.5)$$

$\Omega = 1$ gives a flat space, $\Omega > 1$ a positive curvature and $\Omega < 1$ a negative curvature.

At present, ρ appears to be dominated by matter, the contribution from photons being negligible ($\Omega_r = (4.800 \pm 0.014) \times 10^{-5}$). Ω_ρ is split into contributions from baryonic ($\Omega_B = 0.0456 \pm 0.0016$) and dark matter ($\Omega_{DM} = 0.227 \pm 0.014$). The presence of “cold” (with a negligible velocity dispersion) dark matter – called “dark” because it does not interact electromagnetically with the other components of the cosmic fluid – is well-established by observations of galaxy rotation curves, the X-ray emission of the hot ionized gas in clusters of galaxies and gravitational lensing surveys. As for its origin, various candidates predicted by extensions of the Standard Model of particle physics have been proposed, but to date, the question about the nature of dark matter is awaiting a definitive answer.

The dominant contribution to the present energy budget of the Universe is, however, given by Λ , that is, $\Omega_\Lambda = 0.728^{+0.015}_{-0.016}$. This implies that $\Omega_\Lambda + \Omega_B + \Omega_{DM} = 1$ and the space is flat.

As we go backwards in cosmic time, $R(t)$ decreases and the radiation density increases faster than the density of matter. Therefore, there must have been a moment in the cosmic history when the Universe was radiation dominated; the cosmic time t_E of matter-radiation equality is of the order of 10^5 years. Going back to even earlier cosmic times, it is clear that the Universe must have started from a singular state with $R = 0$ and $\rho = \infty$ at $t = 0$. Present estimates of the matter and Λ density coupled to the equations for the evolution of $R(t)$ provide a value of the Hubble constant $H_0 = 70.4^{+1.3}_{-1.4} \text{ km Mpc}^{-1} \text{ s}^{-1}$ and an age of the Universe $t_U = 13.75 \pm 0.11 \text{ Gyr}$.

Now, reversing the arrow of cosmic time, as the Universe expands and cools from the initial singularity during the initial radiation dominated era, a small amount

1) An interesting comparison of various points of view on this issue can be found in [2].

of some light elements (mainly D, ^3He , ^4He , ^7Li) is produced when the temperature evolves from $T \sim 10^9$ K down to 3×10^7 K. The amount of light nuclei produced depends on the baryon density and the expansion (i.e. cooling) rate. Calculations of cosmological nucleosynthesis – assuming three neutrino species with mass much smaller than 1 MeV – provide, for the present estimate of the baryon density, a primordial He mass fraction $Y_p = 0.2487 \pm 0.0002$, and number abundance ratios $(\text{D}/\text{H})_p = (2.52 \pm 0.17) \times 10^{-5}$, $(^3\text{He}/\text{H})_p = (1.03 \pm 0.03) \times 10^{-5}$, $(\text{Li}/\text{H})_p = 5.12^{+0.71}_{-0.62} 10^{-10}$ for D, ^3He and ^7Li , respectively [3, 4].

When the temperature drops below the ionization energy of hydrogen (13.6 eV), the ionization fraction, however, stays close to one due to the large number of photons over baryons (photons dominate by number, although matter dominates energetically and therefore gravitationally). The number of photons in the high energy tail of the black body spectrum is high enough to keep the matter fully ionized. Eventually, the temperature and therefore the number density of sufficiently energetic photons drops so low that recombination prevails. It is at this time, $\sim 10^{5.5}$ years after the singularity (i.e. when $T \sim 4000$ K), that the first atoms form. The resulting dearth of free electrons has the consequence of reducing the efficiency of electron scattering, so that matter and radiation decouple. From this moment on, the temperatures of radiation and matter become different and start to evolve separately; radiation does not interact any longer with matter and can travel undisturbed through space. The radiation temperature T_r is reduced according to $T_r \propto R(t)^{-1}$, and the blackbody spectrum it had at decoupling is preserved. This blackbody radiation, largely homogeneous and isotropic (because of the cosmological principle) with a temperature T_r of ~ 2.73 K is the theoretical counterpart of the CMB.

If the Universe was perfectly isotropic and homogeneous, no structures would have formed with time. However, in the case of inhomogeneities, regions denser than the background tend to contract and get denser still, inducing a growth of the initial perturbation. In 1970, Peebles, Yu, Sunyaev and Zel'dovich predicted that these inhomogeneities had to be imprinted in the CMB as the tiny temperature fluctuations that have been recently detected (they are of the order of $\Delta T/T \approx 10^{-5}$). Fluctuations of the local density of baryonic matter would have behaved as sound waves (with their fundamental mode plus overtones) in the cosmic fluid before recombination, with the photons (to which baryons were tightly coupled before recombination) providing the restoring force. At recombination, the photons started to travel for the first time unimpeded through space; photons released from denser, hotter regions were more energetic than photons released from more rarefied regions. This temperature differences were thus frozen into the CMB at recombination and are detected today. Most importantly, the amplitude and location of the peaks in the power spectrum of these temperature fluctuations are closely related to a number of cosmological parameters (for more details see, for example, the discussion in [5]); in particular, the location of the first peak is mainly related to the geometry of the tridimensional space, whereas the ratio of the heights of the first to second peak is strongly dependent on Ω_B . Also, the values of the Hubble constant and of the cosmological constant affect both location and ampli-

tudes of the peaks, albeit with different sensitivities. Observations show that the fluctuations are consistent with a Gaussian random field and the power spectrum is close to scale invariant, that is, $P(k) \propto k^{n_s}$ with $n_s = 0.963 \pm 0.012$ ($n_s = 1$ for a scale-invariant spectrum).

The widely accepted idea about their origin relates to the so-called inflationary paradigm that can, in principle, explain why $\Omega = 1$ and solve the so-called horizon problem, that is, why the CMB across the sky is to a very good approximation isotropic, even though the size of the region causally connected at decoupling corresponds to about only one degree in the sky today.

The central idea envisages a period in the early Universe where a term \mathcal{A}_{inf} originated by a hypothetical quantum scalar field analogous to the cosmological constant dominates Eq. (1.4). This can be rewritten as

$$H(t)^2 = \frac{\mathcal{A}_{\text{inf}}}{3} \quad (1.6)$$

and its solution, assuming a constant \mathcal{A}_{inf} , is

$$R(t) = R(t_i)e^{\sqrt{\mathcal{A}_{\text{inf}}/3}t} = R_i e^{H(t)t} \quad (1.7)$$

if t is much larger than the cosmic time $t = t_{\text{inf}}$ of the beginning of the \mathcal{A}_{inf} dominated epoch. Provided this exponential expansion (inflation) is long enough, Ω is driven towards one, irrespective of its initial value. Moreover, during inflation, a very small patch of the Universe can grow to enormous dimensions, so that the isotropy of the CMB temperature we see today, arose from a very small causally connected region that underwent an inflationary growth. An expansion by a factor of $\approx 10^{30}$ solves both the flatness and horizon problem without invoking *ad hoc* initial conditions. The quantum field that originated \mathcal{A}_{inf} is expected to experience quantum fluctuations that were stretched by the inflation to the scales we see imprinted in the CMB. The general belief is that inflation occurred when the strong force separated from the electroweak one, at about $t = 10^{-35}$ s, and lasted until about $t = 10^{-32}$ s.

1.1

Galaxy Formation

Starting from the Λ CDM cosmological model, one of the main problems in modern astrophysics research is to understand how a galaxy forms and evolves [6, 7]. Here, we will just summarize the main concepts. The basic idea underpinning the currently most accepted paradigm of galaxy formation is that cosmic structures grow through the mechanism of gravitational instability starting from the pattern of density fluctuations imprinted in the CMB. The dark matter component, having no pressure, begins to collapse well before the baryonic matter, and the primordial density fluctuations will grow. The early evolution of this dissipationless (no energy can be lost through electromagnetic interactions) growth is described by the linear

perturbation theory. Once the perturbations become non-linear, their evolution is modelled using N -body simulations. The final result of the non-linear evolution of a dark matter density fluctuation is the formation of a dark matter halo, an approximately stable state supported by the random motions of the dark matter particles. In standard Λ CDM cosmology, the first haloes form from the smallest scale fluctuations, and are followed by successive merging episodes that produce increasingly more massive structures. The baryons are dragged along by the dark matter that dominates gravity, and the haloes are therefore expected to accrete baryons, so that the individual galaxies we see can be interpreted as the product of the evolution of baryonic matter nested inside a much larger halo of CDM. The efficiency of the accretion process will depend on the depth of halo potential well, and on the pressure of the baryons. Therefore, a complete description of the formation and evolution of galaxies requires a detailed description of the evolution of the dissipative baryons, that is, their accretion, heating, cooling, the associated star formation processes, the chemical evolution, the effect of halo merging on the baryonic component.

Overall, at any given cosmic time, matter is distributed over structures spanning many decades in mass, and growth is driven by merging between haloes of similar mass, by accretion of much less massive haloes and diffuse material, and by destruction by infall onto larger haloes (hence, the name of “hierarchical merging” scenario). A crucial point is that galaxy morphology may be a transient phenomenon and that the different types of galaxies we observe nowadays (the Hubble sequence) reflect the variety of accretion histories. As an example, this scenario envisages that baryons falling smoothly into the potential wells of dark matter haloes produce disks, whereas spheroids (bulges of disk galaxies and isolated elliptical galaxies) are the products of major (i.e. between haloes of similar mass) merger events whereby disks are mixed violently on short timescales, and a burst of star formation depletes substantially the gas content of the merging disks. Smooth accretion of intergalactic gas on spheroids appears then to be able to produce a typical present-day disk galaxy, for example, a rotationally supported disk of gas and young stars and a centrally concentrated bulge system of old stars.

One of the major difficulties in modelling from first principles how galaxies form and evolve is related to the physics that drives the evolution of the baryonic component, that is, gas cooling in dark matter haloes, star formation, chemical evolution and feedback mechanisms that either remove cold gas from a disk or suppress gas cooling. These processes, sometimes labelled “gastrophysics”, are still poorly understood in a galactic context and prescriptions that contain free parameters are employed. These parameters are fixed by demanding that models reproduce sets of available observations, typically at low redshifts. A powerful way to provide strong independent constraints on galaxy formation models in general, and on “gastrophysics” in particular, is to determine star formation histories of stellar populations in galaxies using methods from stellar evolution theory.

A wide range of techniques developed in the last decades make use of stellar evolution models to estimate distances, ages, star formation and chemical evolution histories of galaxies. It is these techniques, the related uncertainties and their future developments that we are going to discuss in detail in the following chapters,

beginning with their theoretical foundations grounded in stellar evolution theory. We will, at the same time, discuss the use of these methods to determine the star formation and chemical evolution histories of old, local stellar populations.

Although observations at high redshift are certainly a more direct way of looking at the formation of galaxies, these objects are very faint and one can derive a more limited amount of information compared to that obtained from nearby galaxies. Stellar populations in the nearby Universe can be studied in much greater detail and provide a view of galaxy formation and evolution that is complementary to that obtained from high redshift data. Also, observations and analyses of the oldest local stellar populations provide completely independent powerful tests and constraints to the overall cosmological model.

We will use a somewhat arbitrary definition of the nearby Universe, one that often only includes those stellar systems resolvable into individual stars. Here, we will also discuss methods for unresolved stellar populations, and their use to study stellar populations at low redshifts corresponding to look-back times that are a negligible fraction of the age of the Universe.

Our definition of old stellar population comes from stellar evolution theory. We denote as “old” all stellar systems harbouring objects with mass below $\approx 2.0 M_{\odot}$, that is, those stars that undergo electron degeneracy in their He-core at the end of the main sequence (MS) phase, plus remnants of more massive objects. Observationally, the colour–magnitude–diagram (CMD) of these populations is characterized by the presence of a well-defined red giant branch (RGB) sequence. In terms of ages, our definition of old populations implies values above ≈ 1 Gyr, that is, these stars are the fossil record (fossil in the sense that their observables are the result of the past star formation history) of the development of cosmic structures over more than 90 % of cosmic evolution.

1.2

Decoding the Fossil Records: Photometric and Spectroscopic Diagnostics

The amount of evolutionary information we can gather from a stellar population is encoded in the radiation emitted by its stars. A population that is resolved observationally into its individual constituents is denoted as “resolved”, while with an “unresolved” stellar population, we denote a system from which we can only observe the integrated light, that is, the sum of the contribution of all its components.

In the case of resolved populations, one can obtain high-resolution spectra – resolution of the order of $\approx 0.1 \text{ \AA}$, most often in the visible wavelength range – of individual stars, that allow the determination of photospheric abundances of several chemical elements using model atmosphere calculations. These abundances provide constraints on the initial chemical composition of the star. Photometric observations through broadband filters (i.e. Johnson–Cousins, Sloan, WFC3, 2MASS) with passbands of order $\approx 10^3 \text{ \AA}$, typically spanning the wavelength range from near-ultraviolet (near-UV) to near-infrared (near-IR), are used to produce CMDs. These diagrams are the main tool to constrain ages, star formation and chemical

evolution histories – this latter in conjunction with estimates from spectroscopy, if/when available – of resolved stellar populations. Intermediate band photometric filters (i.e. Strömgren, DDO, Walraven) with passbands of order $\approx 10^2 \text{ \AA}$ have been devised to derive indices that are particularly sensitive to some specific stellar property, like surface gravity or metallicity (e.g. the indices c_1 and m_1 in the Strömgren system). Narrow band systems – passbands of order $\approx 10 \text{ \AA}$ – also exist (i.e. Oke, Wing). For example, individual bands in the Wing systems are sensitive to CaH, CN, TiO or VO.²⁾

As for unresolved stellar populations, integrated photometry typically in broad-band photometric systems provides colour–colour diagrams or – when measurements in several bands are available – a very low-resolution spectral energy distribution (SED) that can be used to constrain ages and metal content of the parent populations. Integrated spectra with resolution of $\approx 1\text{--}10 \text{ \AA}$ can be used to infer ages and, in principle, detailed individual abundances of several chemical species.

Figure 1.1 displays some examples of photometric and spectroscopic data for resolved and unresolved populations.

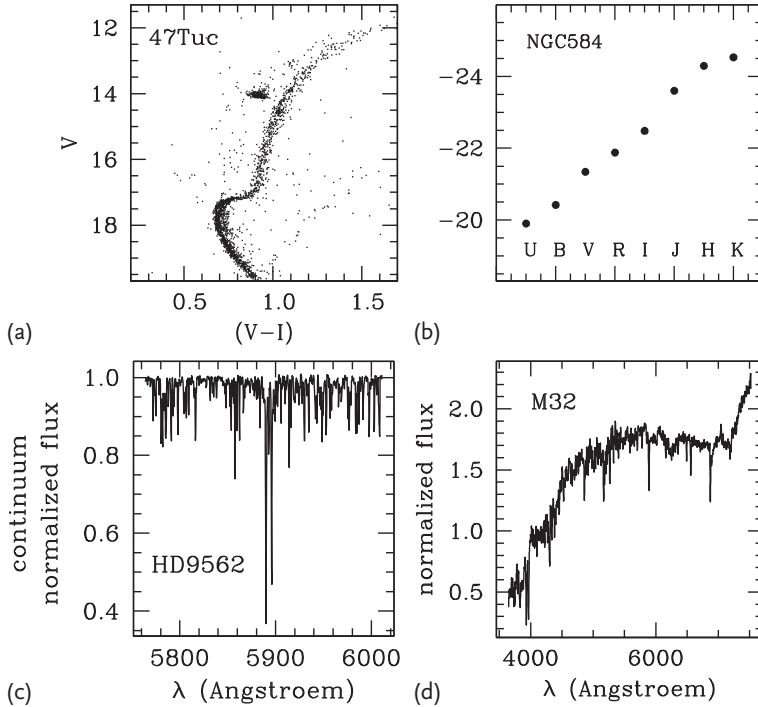


Figure 1.1 (a) A CMD of the Galactic globular cluster 47Tuc [10]. (b) Integrated $UBVR I J H K$ magnitudes of the elliptical galaxy NGC584 [11]. (c) Portion of the spec-

trum of the star HD9562 [12]. (d) Integrated spectrum of the dwarf elliptical galaxy M32 [13]. The fluxes are normalized to the observed flux at 4000 \AA .

2) For an exhaustive review of standard photometric systems and their properties, see [9].

1.3

Decoding the Fossil Record: the Tools

Observed CMDs of resolved populations, SED, colour–colour diagrams, integrated spectra of unresolved populations can be interpreted in terms of evolutionary properties of the parent stars by applying results from stellar evolution theory.

1.3.1

Theoretical Stellar Models, Tracks, Isochrones

The solution of the equations of stellar structure provides a stellar evolution model, that is, the run of physical and chemical quantities from the centre to the photosphere of a star of given initial mass and initial chemical composition, and their evolution with time. It is common practice in stellar astrophysics to specify the initial chemical composition of stellar models by means of the symbols X , Y and Z . They denote the mass fractions of hydrogen, helium and all other elements heavier than helium (called metals, hence Z is also called the metallicity of the star) respectively; these three parameters are related through the normalization $X + Y + Z = 1$. For the metals, the distribution of the individual fractional abundances has to be specified.

This is a convenient choice from the theoretical point of view, though it is not directly related to what is determined from stellar spectroscopy. The helium abundance, for example, cannot be determined for all stars since low-mass objects are generally too cool to show helium spectral lines, and the metal abundances are usually determined differentially with respect to the Sun. The traditional metal abundance indicator is the quantity $[\text{Fe}/\text{H}] \equiv \log [N(\text{Fe})/N(\text{H})]_{\star} - \log [N(\text{Fe})/N(\text{H})]_{\odot}$, that is, the difference of the logarithm of the Fe/H number abundance ratios observed in the atmosphere of the target star and in the solar one. If one assumes that the solar heavy element distribution is universal, the conversion from Z to $[\text{Fe}/\text{H}]$ is given by

$$[\text{Fe}/\text{H}] = \log \left(\frac{Z}{X} \right)_{\star} - \log \left(\frac{Z}{X} \right)_{\odot} \quad (1.8)$$

If one relaxes the assumption of a universal scaled-solar heavy element distribution, the correspondence between $[\text{Fe}/\text{H}]$ and X , Y , Z obviously changes because the ratio between the iron abundance and Z is different than in the Sun. In this case, one can still use Eq. (1.8), provided that the left-hand side denotes the ratio of the “total” abundance of metals to hydrogen

$$[M/\text{H}] = \log \left(\frac{Z}{X} \right)_{\star} - \log \left(\frac{Z}{X} \right)_{\odot} \quad (1.9)$$

A basic working tool in stellar evolution studies is the Hertzsprung–Russell diagram (HRD), a plot of a star bolometric luminosity versus its effective temperature – both outcomes of stellar evolution calculations – that will be widely used in

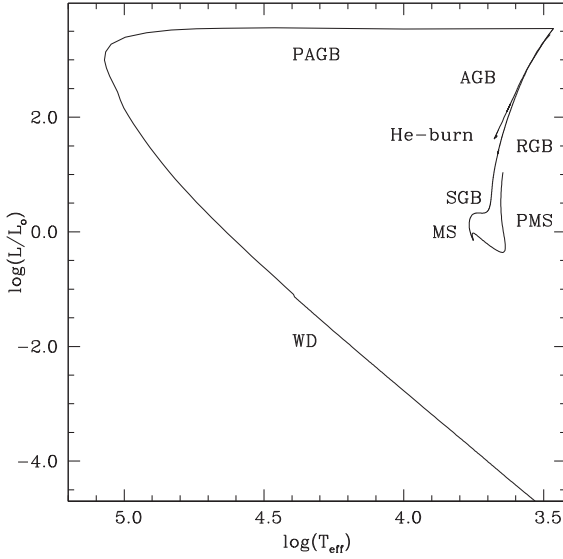


Figure 1.2 Theoretical HRD for the evolution of the Sun. All major evolutionary phases are labelled (see text for details).

the next chapters. The evolution of a stellar model in the HRD is denoted as the “stellar track”.

Figure 1.2 displays the complete theoretical HRD, from birth to the final evolutionary stage, for the Sun. All main evolutionary stages of low-mass stars discussed in the next chapters are covered in this diagram. The starting point of the evolution shown in Figure 1.2 is the pre-main sequence (PMS) phase, where the star is convective and evolves vertically in the HRD along its so-called Hayashi track driven by gravitational contraction according to the virial theorem, until a radiative core forms and eventually H-burning ignites in the central regions. At this stage, the evolution slows down, while H is converted into He in the core, during what is denoted as the main sequence (MS) phase. It is the longest evolutionary phase and as a consequence, the number of H-burning stars which can be observed in a given population is much larger than the number of stars in any other phase. When the central H is exhausted, the H-burning shifts to a narrow shell around the pure He-core left over by the central H-burning, and the subgiant branch phase (SGB) starts. During the SGB evolution, the He-core undergoes electron degeneracy, the external layers expand and the photosphere gets cooler, until the model – by now with a very deep convective envelope – reaches its red giant branch (RGB) location, an approximately vertical sequence in the HRD. During SGB and RGB evolution, the He-core grows steadily in mass due to fresh He deposited by the outward moving (in terms of mass layers) H-burning shell, and correspondingly, the surface luminosity increases. Along the RGB, mass loss processes are also efficient, and reduce the mass of the convective envelope.

When the electron degenerate core reaches a mass of about $0.47 M_{\odot}$, He-burning ignites in the core (He flash), the electron degeneracy is lifted and the star begins a phase of quiescent central He-burning (labelled as He-burn in Figure 1.2) at a much lower luminosity compared to the end termination of the RGB. The precise value of T_{eff} is determined by the amount of mass left in the envelope, T_{eff} getting higher with decreasing envelope mass (more efficient RGB mass loss). In metal-poor systems like Galactic globular clusters (GCs), the central He-burning stage appears as an extended, more or less horizontal sequence in the CMD at visible wavelengths, and it's called the Horizontal Branch (HB). During this central He-burning phase, the H-burning shell is still active, and when He is exhausted in the core, shell burning provides the energy necessary to maintain hydrostatic equilibrium.

The model now has a C and O core left over by the central He-burning that becomes electron degenerate, marking the beginning of the asymptotic giant branch (AGB) phase. During the AGB evolution, H and He shell burning are never active at the same time, instead they take turns at producing the nuclear energy necessary to maintain hydrostatic equilibrium through a series of so-called thermal pulses (TPs). The AGB sequence practically overlaps with the RGB in the HRD, and the evolution is towards increasing luminosity because of the mass increase of the CO-core due to the He-burning shell. Mass loss is again very effective in reducing the envelope mass. When the envelope mass (reduced by both the growth of the CO-core and mass loss from the photosphere) is reduced to $\approx 0.01 M_{\odot}$, the model starts its post AGB (PAGB) phase, moving towards higher T_{eff} at constant luminosity, fixed by the value of the CO-core mass, equal to about $0.54 M_{\odot}$, with some residual shell burning.

The PAGB phase terminates when the model reaches its white dwarf (WD) cooling sequence. From this point on, the evolution is towards lower surface luminosities (and T_{eff}), the energy radiated being the free energy of the non-degenerate ions, while hydrostatic equilibrium is maintained by the pressure of the degenerate electrons.

Stellar tracks of different masses and chemical compositions can be combined to predict the HRD of stars harboured by stellar populations with a generic star formation and chemical evolution history. The most elementary stellar population, usually denoted as simple stellar population (SSP), is made of objects born at the same time in a burst of star formation activity of negligible duration, with the same initial chemical composition. Any population with an arbitrarily complex evolutionary history can be reduced to a linear combination of several SSPs.

The theoretical HRD of a SSP is called isochrone. Consider a set of evolutionary tracks of stars with the same initial chemical composition and various initial masses; different points along an individual track correspond to different values of the time t_{tr} and the same initial mass. An isochrone of age t is the line in the HRD that connects the points belonging to the various tracks (one point per track) where $t_{\text{tr}} = t$. This means that when we move along an isochrone, time is constant. However, the value of the initial mass of the star at each point is changing, that is, increasing towards more advanced evolutionary stages. A generic point along

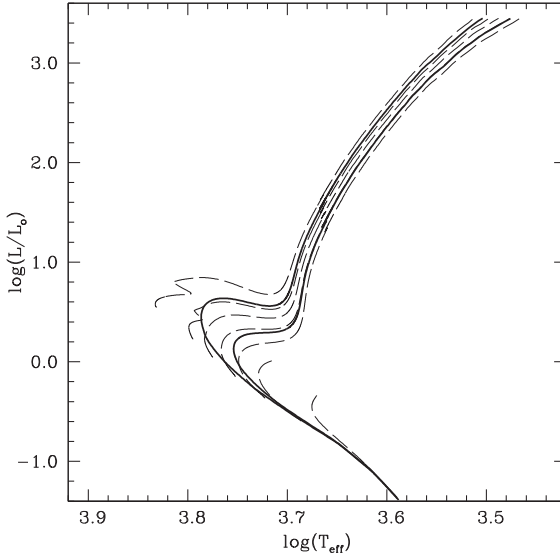


Figure 1.3 Isochrones for 5 and 13 Gyr and solar initial chemical composition (thick solid lines) overimposed on a set of stellar tracks for the same initial chemical composition

(thin-dashed lines). We display in order of increasing luminosities along the MS, tracks for $0.6, 0.8, 0.9, 1.0, 1.1, 1.2$ and $1.4 M_{\odot}$.

an isochrone of age t is therefore determined by three quantities: bolometric luminosity, effective temperature and value of the evolving mass. From these three parameters, one can easily derive additional quantities like the radius and surface gravity. It is also straightforward to associate to each point along an isochrone the expected surface chemical abundances – taken from the underlying grid of stellar evolution models – to be compared with spectroscopic measurements.

If mass loss processes are included in the individual stellar tracks – as we have briefly seen before, mass loss is very efficient during the RGB and AGB evolution of low-mass stars – the situation is only slightly more complicated because along each track the total mass is changing with time. The procedure to compute the isochrones is the same, that is, one connects the points of equal age along tracks with various initial masses. However, the value of the mass evolving at a given point along the isochrone is now smaller than the initial mass of the parent track.

Figure 1.3 shows, as an example, two isochrones for ages equal to 5 and 13 Gyr, respectively, and the solar initial chemical composition, that cover the evolutionary phases from the MS to the He flash. Notice the large mass range spanned by the MS phase, whereas the SGB and RGB stages (this is true for all post-MS phases but the final WD stage) are populated by objects with almost the same mass, equal to the value at the termination of the MS (the so-called turn off point – TO). This is a consequence of their much shorter evolutionary timescales, compared to MS lifetimes.

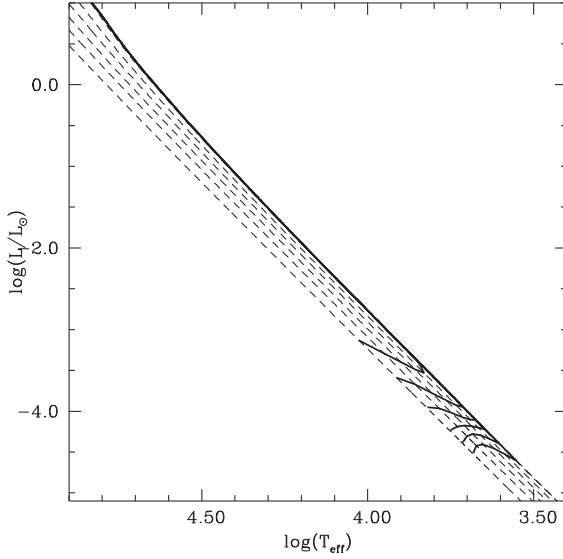


Figure 1.4 Isochrones for 2, 4, 6, 8, 10 and 12 Gyr (solid lines) overimposed on a set of WD cooling tracks with masses between 0.54 and $1.0 M_{\odot}$ (dashed lines).

Representative isochrones for the final WD stages are shown in Figure 1.4. Along a WD isochrone, it is the sum of the WD cooling age plus the progenitor age at the end of the TP phase that stays constant. Obviously, a fundamental ingredient to calculate WD isochrones is the relationship between the mass of the progenitor on the MS (initial mass) and its final WD mass (initial-final mass relation – IFMR – see Chapter 6 for details). Due to the fast cooling times at high T_{eff} , the bright section of a WD isochrone of fixed age is populated by objects with approximately the same mass, corresponding approximately to the final WD mass of stars that have just left the TP phase. One can also notice that all isochrones in Figure 1.4 share the same location at bright luminosities because empirical and theoretical IFMRs predict essentially the same WD mass ($\sim 0.55 M_{\odot}$) for all low-mass stars. At the bottom end of the sequence, one recovers the progeny of more massive intermediate-mass stars that have left the TP phase earlier. This explains the sudden increase of T_{eff} (lower radii) since the more massive progenitors produce WDs of increasing mass, and hence lower radius.

Once a generic isochrone of a given age and initial chemical composition is computed, it can be transferred to an observational CMD, that is, the plot of a star magnitude in a given photometric band versus a colour index. To predict magnitudes in a generic photometric system, one needs to assign a spectrum to each point along the isochrone, making use of model atmosphere calculations.

A model atmosphere describes the physical and chemical structure of a stellar atmosphere and the transfer of radiation from the photosphere into interstellar space. It is defined (at least in the plane-parallel approximation) by three quantities: the value of T_{eff} , the surface gravity g and the photospheric chemical composition.

Interpolation among a suitable grid of spectra obtained from model atmosphere calculations provides spectra to assign to each point along the isochrone.

From a given spectrum, it is straightforward to compute bolometric corrections BC_A to a generic filter A from the following equation:³⁾

$$BC_A = M_{\text{bol},\odot} - 2.5 \log \left[4\pi(10p c)^2 \frac{a c T_{\text{eff}}^4}{4L_{\odot}} \right] + 2.5 \log \left(\frac{\int_{\lambda_1}^{\lambda_2} F_{\lambda} S_{\lambda} d\lambda}{\int_{\lambda_1}^{\lambda_2} f_{\lambda}^0 S_{\lambda} d\lambda} \right) - m_A^0 \quad (1.10)$$

Here, $M_{\text{bol},\odot}$ is the bolometric magnitude of the Sun, F_{λ} is the model spectrum (i.e. from model atmosphere calculations), S_{λ} is the response function of the photometric filter (a measure of the efficiency of photon detection within the filter wavelength range) that covers the wavelength range between λ_1 and λ_2 , f_{λ}^0 denotes the reference spectrum that produces a known apparent magnitude m_A^0 (for example, the spectrum of Vega, or a spectrum of constant flux density per unit frequency for the ABmag system. In both cases, the apparent magnitude m_A^0 is usually set to zero). From BC_A , one can then obtain the magnitude M_A from

$$M_A \equiv M_{\text{bol}} - BC_A \quad (1.11)$$

where $M_{\text{bol}} = M_{\text{bol},\odot} - 2.5 \log(L/L_{\odot})$. The value of L_{\odot} is known, and once the bolometric magnitude of the Sun is fixed (e.g. $M_{\text{bol},\odot} = 4.74$ [14]), what is left in order to convert T_{eff} and the bolometric luminosity L into magnitudes is the choice of f_{λ}^0 and m_A^0 , the so-called “zero points” of the photometric system.

The very popular Johnson–Cousins and the Hubble Space Telescope HST/WFPC2 VEGAmag systems, for example, make use of the star Vega to fix the zero points, assuming that the apparent V magnitude of Vega and all its colour indices are equal to zero. The Sloan system instead uses a zero point flux $f_{\nu}^0 = 3.63110^{-20} \text{ erg s}^{-1} \text{ cm}^{-2} \text{ Hz}^{-1}$ that gives $m_A^0 = 0$ at all frequencies (see [15] for details about zero points of several photometric systems). Figure 1.5 displays the response function of a few widely used filters;⁴⁾ a theoretical low-resolution spectrum of Vega is overimposed, for the sake of comparison.

The transformation from theoretical luminosity and T_{eff} to observed magnitudes and colour indices has been described assuming up to now that F_{λ} at the stellar surface is obtained from the appropriate theoretical model atmospheres. It is, however, known that current theoretical model atmospheres suffer from at least two main shortcomings:

- Broad-band colours of stars with solar chemical compositions appear to be reasonably reproduced, but many spectral lines predicted by the models are not

3) The terms in the two integrals are formally correct if the calibration of the photometric system is based on energy-amplifier devices; they need to be multiplied by λ when the calibration is based on photon-counting devices like CCDs. The difference between

these two types of integrations is usually very small.

4) A complete database of photometric filters can be found at <http://ulisse.pd.astro.it/Astro/ADPS/> (accessed 22 January 2013).

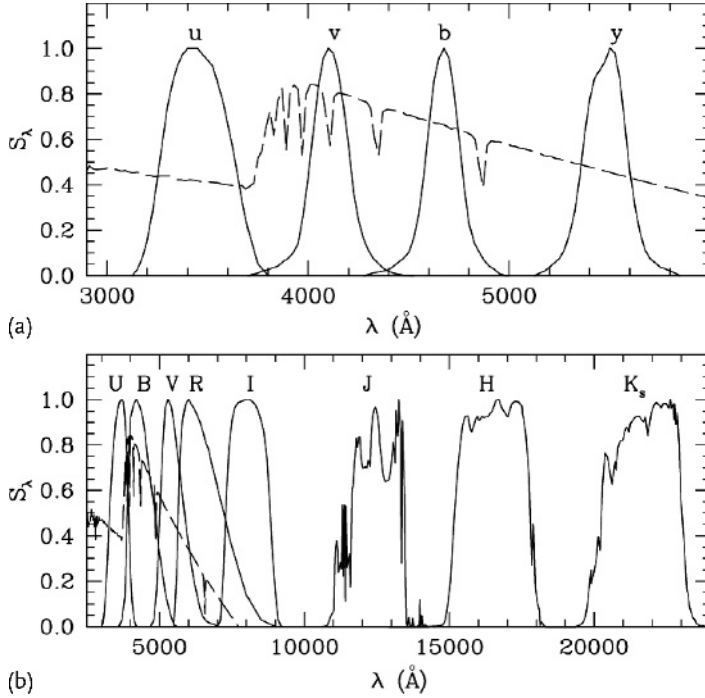


Figure 1.5 Response functions of the $uvby$ Strömgren photometric filters (a), Johnson–Cousins $UBVRI$ and 2MASS JHK_s (b). Overimposed is a theoretical spectrum of the star Vega (dashed line) [16].

observed in the Sun, and also the relative strength of several lines is not well-reproduced. This affects intermediate- and narrow-band filters in which individual metal lines can significantly affect the bolometric corrections.

- In convective model atmospheres, the energy transport is usually treated with the mixing length theory (see next chapter); this approximation introduces an uncertainty in the predicted spectra, and hence bolometric corrections and colour indices. Recent two- and tridimensional hydrodynamical simulations of stellar model atmospheres are addressing this issue, but they have not produced yet libraries of stellar spectra that cover all the relevant evolutionary phases, mass ranges and chemical compositions.

These shortcomings cause an uncertainty of possibly a few hundredths of a magnitude on the BC_A values. An alternative solution is to use empirical spectra of a sample of nearby stars with independently determined T_{eff} , gravities and chemical composition. A problem with this approach is that stars for which empirical T_{eff} values can be determined are local objects that cover a fairly narrow combined range of chemical compositions, masses and evolutionary phases (reflecting the local population of the Galactic disk) and would not allow a complete modelling of different stellar populations.

1.3.2

Luminosity Functions, Synthetic CMDs

The CMD of an isochrone only provides a morphological counterpart to the observed CMDs of resolved stellar populations, for it does not give any information about the number of objects expected along the different branches of the observational diagrams. As we will see in the next chapters, just using isochrones is enough to constrain ages and initial chemical compositions of resolved SSPs. However, additional information coming from star counts must be accounted for when trying to disentangle the star formation and chemical evolution history of more complex stellar populations.

Given that each point along an isochrone corresponds to a specific evolutionary stage of a model of initial mass M , assuming a stellar initial mass function (IMF) that provides the number of stars dN born with mass between M and $M + dM$, will also provide the number of objects populating a generic interval between two consecutive points along the isochrone. For an IMF of the standard form $dN = C M^{-x} dM$, the normalization constant C can be fixed by specifying either the total mass (M_t) or the total number (N_t) of stars born when the SSP formed. When $x \neq 2$, the value of the constant C is given by

$$C = (2 - x) \frac{M_t}{M_u^{2-x} - M_l^{2-x}} \quad (1.12)$$

where x is the exponent of the IMF, M_u and M_l are, respectively, the upper and lower mass limits of the stellar entire mass spectrum, for example, ~ 0.1 and $\sim 100 M_\odot$. If $x = 2$,

$$C = \frac{M_t}{\ln(M_u/M_l)} \quad (1.13)$$

This normalization guarantees that the total mass of stars formed stays constant, independent of the value of x , but the initial number of stars formed changes with changing value of the slope of the IMF. In the case N_t instead of M_t is given, the previous relationships have to be rewritten as

$$C = (1 - x) \frac{N_t}{M_u^{1-x} - M_l^{1-x}} \quad (1.14)$$

if $x \neq 1$ and

$$C = \frac{N_t}{\ln(M_u/M_l)} \quad (1.15)$$

if $x = 1$.

One way to compare observed star number counts with theory is to use luminosity functions (LFs). One can make use of two types of LFs. The differential LF, for example, the run of the observed star number counts $N(M_A^i)$ in the magnitude range between M_A^i and M_A^{i+1} , as a function of M_A^i , or the cumulative LF, that is,

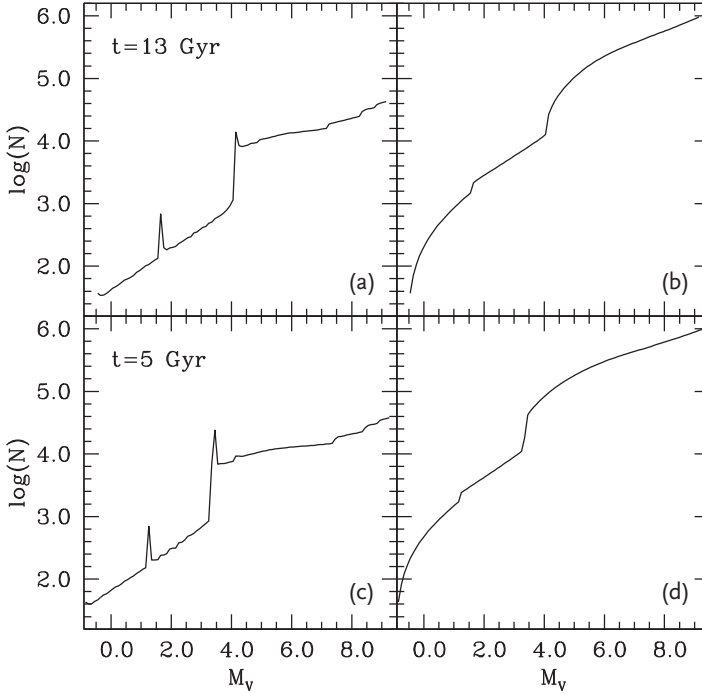


Figure 1.6 Differential (a,c) and cumulative (b,d) LFs for the isochrones displayed in Figure 1.3, computed with a Salpeter IMF and a total population of 10^6 stars.

the run of the number of stars $N(M_A > M_A^i)$ (or $N(M_A < M_A^i)$) with magnitude M_A larger than M_A^i (or lower than M_A^i), as a function of M_A^i itself.

Figure 1.6 displays both the differential and cumulative LF for the two isochrones displayed in Figure 1.3. The normalization constant has been chosen in order to have 10^6 objects along each isochrone. The exponent is $\alpha = -2.35$, the so-called Salpeter IMF [17].

Finally, a synthetic CMD combines both isochrone and the predicted star counts (for a given IMF). Synthetic CMDs can be easily calculated by iterating the following procedure. For a fixed age and initial chemical composition of a SSP (the generalization to complex star formation histories is straightforward), the starting point is to randomly draw a value of the mass M for the synthetic star according to a specified IMF. With this value of M , one interpolates along the appropriate isochrone to determine the magnitude and colour of this synthetic object. Inclusion of photometric errors and unresolved binaries is also straightforward. The magnitude and colour obtained from the isochrone interpolation are modified by adding a value of the photometric error, drawn from a Gaussian (for example) random distribution with σ specified by the data reduction process. A given number of unresolved (non-interacting) binaries or blends of single stars can be included in a similar fashion. To these selected stars (whose mass is denoted as M_{pr}), it is assigned a companion (with the same age and metallicity of M_{pr}) whose mass M_{comp}

is drawn according to

$$M_{\text{comp}} = [\text{ran}(1 - q_c) + q_c] M_{\text{pr}} \quad (1.16)$$

where q_c is the minimum value of the ratio $M_{\text{comp}}/M_{\text{pr}}$, to be chosen. The variable ran is a random number with a flat probability distribution between zero and one, so that the previous relationship provides values of M_{comp} with a uniform distribution between M_{pr} and $q_c M_{\text{pr}}$. The magnitude of the composite object is evaluated by summing up the fluxes of the components; in a generic band A, the magnitude of an unresolved binary is given by $M_A(\text{bin}) = -2.5 \log(10^{-0.4 M_A(1)} + 10^{-0.4 M_A(2)})$, where $M_A(1)$ and $M_A(2)$ are the magnitudes of the two system components M_{pr} and M_{comp} .

It is important to notice that one can also determine theoretical LFs from synthetic CMDs simply by counting the synthetic objects in the appropriate magnitude bins. The main conceptual difference with the “analytical” integration of the IMF along an isochrone described before is that this latter procedure is strictly valid only when the number of stars is formally infinite. The analytical computation implies that all points along an isochrone are smoothly populated by a number of stars that can be equal to just a fraction of unity in case of fast evolutionary phases. However, in real stellar populations (or in synthetic CMDs), the number of objects in a given magnitude bin is either zero or a multiple of unity. When the number of stars harboured by the observed population is not large enough to smoothly sample all evolutionary phases, statistical fluctuations of star counts at a given magnitude will arise, and their extent can be easily evaluated using extensive synthetic CMD simulations.

1.3.3

Stellar Population Synthesis Models

In the case of unresolved stellar systems, photometric and spectroscopic observations can only provide integrated magnitudes, colours and spectra that include the contribution of all the stars belonging to the population. Theoretical predictions of integrated properties of stellar populations are often called “stellar population synthesis” models.

The theoretical counterpart of integrated magnitudes and spectra of SSPs is conceptually easy to determine. Consider a generic CMD of an isochrones of fixed age and initial chemical composition. The integrated magnitude in the photometric band A can be written as the sum of the energy fluxes within the appropriate wavelength range, that is,

$$M_A(t) = \int_{M_l}^{M_u} 10^{-0.4 M_A(M,t)} \Phi(M) dM \quad (1.17)$$

where $\Phi(M) dM$ is the IMF, M_l is the mass of the lowest mass star in the SSP, M_u is the mass of the highest mass star still “alive” in the SSP (remnants’ contribution is negligible), $M_A(M, t)$ is the magnitude of a star of mass M evolving along

the isochrone of age t . Integrated colours follow directly from the same equation applied to two different photometric bands.

Equation (1.17) says that the integrated magnitude is the sum of the individual fluxes (in the appropriate wavelength range) of the stars belonging to the SSP; the IMF gives the number of stars formed with a given mass M , and in the assumption of a universal IMF, the effect of age and chemical composition is included in the term $10^{-0.4M_A(M,t)}$ – for the energy output of a star of mass M and its wavelength distribution depend on both age t and initial chemical composition – and in M_u .

As for the calculation of theoretical integrated spectra, it is easy to realize that the monochromatic integrated flux F_λ received from an unresolved SSP can be written as

$$F_\lambda(t) = \int_{M_l}^{M_u} f_\lambda(M, t) \Phi(M) dM \quad (1.18)$$

where $f_\lambda(M, t)$ is the monochromatic flux emitted by a star of mass M evolving along the isochrone.⁵⁾ From the integrated F_λ , one can obviously determine the integrated magnitude in the generic photometric band A. In fact, if F_λ^{int} is the total integrated flux obtained by adding up the individual fluxes at the stellar surfaces, the generic integrated absolute magnitude M_A will be equal to

$$M_A = -2.5 \log \left(\frac{\int_{\lambda_1}^{\lambda_2} F_\lambda^{\text{int}} S_\lambda d\lambda}{\int_{\lambda_1}^{\lambda_2} f_\lambda^0 S_\lambda d\lambda} \right) + m_A^0 \quad (1.19)$$

As in the case of the computation of LFs, this analytical formalism to determine integrated magnitudes and fluxes is strictly valid only when the number of stars is formally infinite. When the different evolutionary phases are not smoothly sampled, it is possible to make use of synthetic CMDs to easily determine the statistical fluctuations of the integrated properties. One simply needs to add the monochromatic fluxes – or the fluxes within a given photometric passband – assigned to each of the synthetic stars.

5) It is important to notice that, for example, in the case of theoretical stellar spectra (that give energy per unit area), the fluxes $f_i(M, t)$ need to be rescaled appropriately by accounting for the radii of the models, and eventually to a distance of 10 pc if a prediction of the “absolute” flux scale is needed.